Gas dynamics of the pulsed emission of a perfect gas with applications to laser sputtering and to nozzle expansion

Roger Kelly*
IBM Research Division, Thomas J. Watson Research Center, Yorktown Heights, New York 10598
(Received 4 December 1990; revised manuscript received 7 February 1992)

Particles released from a target surface by laser-pulse bombardment normally collide with each other and, as a result, exhibit three limiting categories of gas-dynamic behavior. One possibility, (a), is that the particles pass directly into unsteady adiabatic expansion (UAE), a problem for which an analytical solution already exists. Alternatively, (b), the particles first form a Knudsen layer (KL), then pass into UAE, and are not subject to recondensing at the target surface if the release pulse terminates, or else, (c), the particles go through the same sequence of KL formation and UAE but are subject to recondensing. Closely related to (b) is the behavior of particles that escape into vacuum from a nozzle. We here present an analytical, one-dimensional, continuum solution for case (b) when the release is pulsed. The KL (like the throat of the nozzle) is treated as a boundary condition with a nonzero flow velocity. During the release pulse the solutions take on our previously derived forms for a planar UAE from an infinite reservoir. When the pulse ends (or the nozzle closes), there is an abrupt change of boundary condition from finite to zero flow velocity and from high to intermediate sound speed (thence density); at the same time the flow pattern breaks up into three regions. These analytical results are finally compared with the numerical solution of the flow equations by Knight [AIAA J. **20**, 950 (1982)], with Monte Carlo solution of the Boltzmann equation by Sibold and Urbassek [Phys. Rev. A **43**, 6722 (1991)], and with the explicit nanosecond-time-scale photography of Braren, Casey, and Kelly [Nucl. Instrum. Methods B **58**, 463 (1991)]. The comparison with the Boltzmann equation is particularly important, as the generally good agreement with the flow equations suggests the latter to be useful in spite of being founded on the assumption of persistent local equilibrium.

PACS number(s): 51.10.+y, 79.20.Ds, 47.55.Ea, 47.45.−n

I. INTRODUCTION

The release (i.e., ablation, desorption, sputtering, or vaporization) of particles from a target surface due to the impact of ions, electrons, or photons constitutes an active contemporary field. Applications include surface analysis, surface texturing, thin-film deposition, ion formation for mass spectrometry, fundamental surface studies, and fundamental studies of particle dynamics. Under some circumstances, such as when laser pulses are incident, the emitted particles exhibit prominent gas-dynamic effects because of gas-phase collisions. Three limiting categories of behavior will be recognized in what follows. In the first, (a), the collisions are those appropriate to the escape of gas from a finite reservoir such as a gun, the escape being in the form of an *unsteady adiabatic expansion* (UAE) without a formal *Knudsen layer* (KL) [1,2]. This was termed the "outflow" model [3]. In the second, (b), the collisions are those appropriate when both a KL and UAE are present. In one form of the model the particles are not subject to recondensing at the target surface if the release pulse ends ("effusion" model), but recondensation is readily taken into account. This leads to a third possibility, (c), the "recondensation" model [3]. Closely related to (b) is the behavior of particles that escape into vacuum from a nozzle. We here present an analytical, one-dimensional, continuum solution for case (b) when the release is pulsed. This continues the work begun in [4], where only nonpulsed situations were considered. Still to be developed are the solutions for case (c) when the release is pulsed.

A. Escape into vacuum from a combined KL-UAE or a pulsed nozzle (effusion and recondensation models)

Particles that are released by sputtering from the outer surface of a condensed phase will, when the number of collisions among them is small (roughly 3 [5,6]), form a KL [7–12]. This can be described as the region in which the independently emitted particles come to equilibrium with each other, i.e., become thermalized. For a larger number of collisions the KL "feeds" a UAE [4,13]. In some circumstances, as when there is a nearby sink [7,14], the UAE will evolve into a steady adiabatic flow. More usually it terminates due to the falling density, with the particles then going into free flight [4,15] and, depending on the intent of the experimenter, leading variously to thin-film deposition [16–18], mass spectrometry [19,20], or *time-of-flight* (TOF) measurement [4,11–13]. If the release of particles is pulsed, additional gas-dynamic effects set in, and one must then make a distinction as to whether or not recondensation occurs at the target surface. This leads to the "effusion" and "recondensation" models.

Situations in which a combined KL-UAE plays a role are not confined to the sputtering process. Indeed, the

application to sputtering is very recent [4,11–13], with the historical applications being mainly in connection with effusion or strong vaporization [7,14,21,22]. Closely related are nozzle expansions [23–25], except that here, instead of unit Mach number ($M=1$) occurring at the KL boundary, it occurs at the "throat," i.e., narrowest point, of the nozzle.

From a more fundamental point of view, what this all means is that the released particles (whether sputtered or from a nozzle, and whether continuous or pulsed) do not give simple information on the surface from which they come. Rather they reflect the details of the combined KL-UAE. An important example is a TOF temperature, deduced by analyzing the data as if there were no KL-UAE (Fig. 1 [26]). In data of this type the dependence of the temperature on the angle of observation and on the amount of material removed can be understood both as a gas-dynamic effect and as being intrinsic to the sputtering mechanism, with the relative contributions unestablishable without additional information. This fundamental choice was recognized also by NoorBatcha, Lucchese, and Zeiri [5]: see their "models I, II, and III" in their simulation of earlier work by Cowin *et al.* [27]. It was also recognized by Namiki, Kawai, and Ichigi [26], but has been systematically overlooked in many other cases.

Altogether the following effects, not normally relevant to the sputtering process, can be recognized when a combined KL-UAE forms:

(a) chaotic temperature information as in Fig. 1 [26];

(b) recondensation, such that 18–26 % of the emitted particles return to the target surface if there is a KL [7,8,10] and even more return after the release pulse ends if the system is subject to recondensation;

(c) forward peaking among the particles that do not recondense. Angular dependences similar to $\cos^{25}\theta$ are well known [26,28], even if not always interpreted in gas-dynamic terms [28];

(d) lack of stoichiometry in both (b) and (c) [29];

(e) condensation, i.e., cluster formation, among the particles that leave the surface [30–32]. These clusters had masses $<10\,000$ u. Those seen in other work [17,18] by scanning electron microscopy, on the other hand, were so massive ($>10^{10}$ u) that condensation can be immediately excluded;

(f) shock-wave formation when the release process takes place in an ambient gas [33–36].

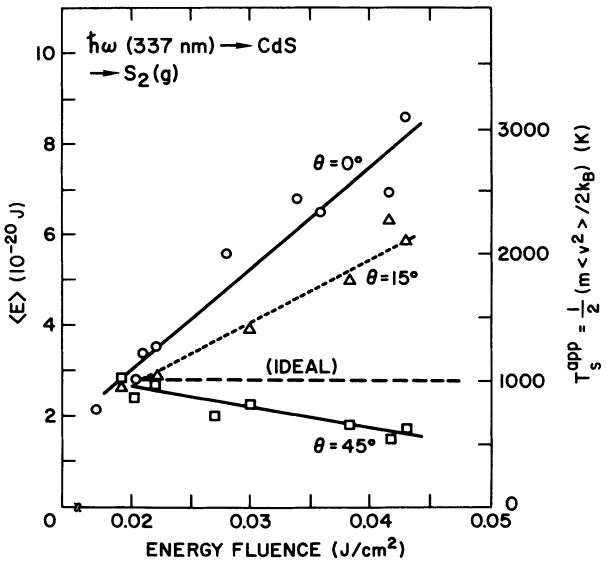

FIG. 1. Examples of apparent time-of-flight (TOF) surface temperatures, i.e., T_s^{app}, vs energy density (fluence) for laser-pulse sputtering of S_2 from CdS. For the lowest energy density only a fraction of a monolayer was removed per pulse, but for the highest densities as much as 1.0 nm, i.e., about 4 monolayers, was removed and gas-dynamic effects should be prominent. The laser pulses had a length of 5 ns and a wavelength of 337 nm (3.68 eV). What is here significant is that the temperatures measured at 0° and 15° increase with energy density, whereas the converse change is observed at 45°. The dashed line labeled "ideal" would apply in the absence of gas-dynamic effects. Due to Namiki, Kawai, and Ichige [26].

B. Escape into vacuum from a finite reservoir (outflow model)

An essential aspect of the argument in the preceding section is that effusionlike release occurs from the outer surface of the target. There are, however, examples in which this is not quite true: heavy-ion sputtering of condensed gases [1,2], laser-pulse sputtering of $YBa_2Cu_3O_{7-x}$ [36], (possibly) laser-pulse sputtering of III-V and II-VI compounds [37], and (possibly) laser-pulse sputtering of polymers [33–36,38,39] or biological tissue [40].

Considering condensed gases, the current view [1,2] is that each incident ion causes first a cascade, then causes a transient temperature increase T^*, and finally, provided the condensed gas achieves the situation $T^*>T_{tc}$, the material rapidly becomes gaseous and outflow in the form of UAE from a finite reservoir occurs. T_{tc} is the thermodynamic critical temperature [21] at which the liquid and gas have the same density. There is no effusionlike release from the target surface and, therefore, no formal KL. The underlying problem is like that of the sudden release of gas from a gun and, although the real dimensionality is axial like a pulsed nozzle, we have achieved reasonable success in treating it as planar [2]. The consequence to TOF studies [4] is in principle as severe as when a KL forms, with all the points (a)–(f) given above remaining valid except (b): such recondensation as occurs would be due not to the KL, but to the on-going return of particles to the back surface of the reservoir [1].

Considering the laser-pulse sputtering of polymers or biological tissue, one of the currently popular models is that the pulse rapidly severs bonds throughout a given depth [34,38]. The resulting gaslike particles then, if this description is valid, began an outflow like that of a condensed gas. This example of outflow is, however, tentative since experiments which might have made a firm distinction (such as those of [36]) were not performed.

C. Concluding remarks

The problem of pulsed particle release when a pure UAE is involved is understood to the extent that, al-

though it is necessary to assume planarity, the solution for atoms is complete [2]. The situation is less satisfactory when there is a combined KL-UAE (or release from a nozzle), since in that case the solutions for continuous release are known [4,41] but those for pulsed release have not yet been discovered. This lack of information for the pulsed release applies equally whether or not there is recondensation at the surface [3]. In what follows we intend to elucidate the problem in two respects: (a) to give a full analytical, one-dimensional, continuum solution of the problem of a combined KL-UAE when the release is pulsed and there is no recondensation, and (b) to discuss relevant numerical [42,43] and experimental [33–36,40] results. This will include showing a generally good agreement between the Boltzmann equation [43] and the present results.

We will not consider the recent work of Vertes and co-workers [19,20]. They made a numerical treatment of laser-pulse sputtering which in many respects overlapped the present work rather closely. However, the results did not resemble those obtained here, a detail which we attribute in part to energy being deposited in the escaping particles. Our treatment is thus for low laser fluence (J/cm^2) and that of Vertes and co-workers for high fluence.

II. THE BEGINNING OF THE PULSE

A. Situations with a formal KL

We consider here a pulsed beam of bombarding ions, electrons, or photons which is uniform in space and time, and which will in most experimental situations be a photon pulse from a laser. We suppose that at time $t=0$ a pulse begins to strike the target surface and, as a result, particles abruptly begin to be released. The two most common categories of such release are thermal (e.g., with C[44]) and electronic (e.g., with Al_2O_3 [45]).

If the release is thermal, the particle velocities will be distributed as a Maxwellian [8,10] characterized by number density n_s, pressure p_s, temperature T_s, positive velocities (v_x) normal to the surface (s), zero flow velocity u, and zero Mach number M. Although the flow velocity is formally zero, there is an effective flow velocity (u_s), arising because v_x is positive [4], which we will need for a comparison of the present analytical results with the numerical results of Sibold and Urbassek [43] (Sec. VI C):

$$u_s=\langle v_x\rangle=(2k_BT_s/\pi m)^{1/2}=0.797\,88(k_BT_s/m)^{1/2}\ . \tag{1a}$$

If the relapse is electronic, i.e., due to bond breaking, it is less clear what form the velocity distribution will take.

For high enough emitted particle densities, gas-phase collisions will occur, the first stage of which is the KL [7–12] during which the independently emitted particles come to equilibrium with each other. We have summarized the consequences of KL formation previously [4], so here indicate only the final results.

(a) The velocity distribution is probably Maxwellian-like whether the initial release is thermal or electronic [3]. It will be "circular" with one temperature rather than "elliptical" with two temperatures [22].

(b) The particles acquire a lower number density n_K, pressure p_K, and temperature T_K. For atoms with $\gamma=\frac{5}{3}$

TABLE I. Notation for density, flow velocity, kinetic velocity, pressure, and temperature as used in the present work and in closely related articles.

Quantity	Present usage; also [3,4]	[43]	[7]	[10]
Density of saturated vapor at target surface[a]	n_s or ρ_s	n_v	n_L	ρ_L
Density of emitted vapor at target surface ("real" density)	$n_s/2$ or $\rho_s/2$	$n_0=n_v/2$	$n_L/2$	$\rho_L/2$
Density of emitted vapor at KL boundary	n_K or ρ_K	n_K	n_∞	ρ_M
Effective flow velocity at target surface[b]	$u_s=\langle v_x\rangle=\langle v\rangle/2$	$v_0=v_T/2$		
Arithmetical mean kinetic velocity[c]	$\langle v\rangle$	v_T		
Flow velocity at KL boundary	u_K	u_K	u_∞	u_M
Pressure of saturated as well as emitted vapor at target surface	p_s	p_v	p_L	p_L
Pressure of emitted vapor at KL boundary	p_K		p_∞	p_M
Temperature of saturated as well as emitted vapor at target surface	T_s	T_0	T_L	T_L
Temperature of emitted vapor at KL boundary	T_K	T_K	T_∞	T_M

[a] n is a number density and ρ is a mass density, the interrelation being $\rho=mn$.
[b] $\langle v_x\rangle$ is proportional to $\int dv_x v_x \exp(-mv_x^2/2k_BT)$, where v_x is the x component of velocity.
[c] $\langle v\rangle$ is proportional to $\int dv\, v^3\exp(-mv^2/2k_BT)$, where v is the scalar velocity.

TABLE II. Comparison of the time-diameter ratio for laser-pulse sputtering and for pulsed-nozzle expansion.

Situation	Release time (μs)	Release diameter (mm)	Time/diameter (μs/mm)	Reference
Excimer laser	0.020	0.75	0.03	[33]
	0.020	0.97	0.02	[34]
	0.020	0.030	0.7	[58]
Other laser	100	0.12	800	[59]
	1500	0.32	5000	[59]
Nozzle	20	0.6	30	[47]
	1000	0.2	5000	[48]

we have $n_K/n_s=0.3082$, $T_K/T_s=0.669\,12$, and $p_K/p_s=0.3082\times0.669\,12=0.2062$ [7,8,10]. Here $\gamma=C_p/C_V$ is the heat capacity ratio ("adiabatic index").

(c) The normal velocity v_x is replaced by v_x-u_K, where u_K is the positive flow velocity and v_x can be both negative and positive.

(d) u_K is given by

$$u_K=a_K=(\gamma k_B T_K/m)^{1/2}=1.0560(k_B T_s/m)^{1/2}\ , \tag{1b}$$

where a_K is the sound speed and m is the particle mass. (The number appearing in this equation was previously [4] written incorrectly as 1.046 instead of 1.0560.)

(e) The Mach number, defined by $M=u/a$, is given by $M=1$.

Because of the potential for confusion, the present notation is compared with that of other work in Appendix A (Table I).

B. The pulsed nozzle

A pulsed nozzle expansion is similar in spirit to the pulsed sputtering of particles from the outer surface of a target. Although it lacks a formal KL, there is instead, in the "throat" of the nozzle, a region with $M=1$. Differences include the fact that a nozzle expansion is not initiated by the simple arrival at the target of a laser pulse, but rather requires the gas to flow roughly one nozzle diameter (1–4 μs [15,46]). It differs more profoundly in that the nozzle pulse length is typically 10–10 000 μs [46–48] compared with 10–30 ns for an excimer-laser pulse. Since the diameters of the released material are similar, this means that the length-diameter ratio is 10^3–10^6 times greater for a nozzle expansion and the released material is therefore very much more extended in space. This can also be shown by comparing values of the time-diameter ratio (Table II). As a result the geometry will tend to be axial rather than planar [23–25].

III. THE FLOW PHASE OF THE PULSE ($0\le t\le\tau_r$)

A. The flow equations

We have proposed previously [4,13], following the example shown in numerical calculations by Knight [42], that the particles released into a vacuum by a pulsed bombardment, once the condition $M=1$ is established and Eq. (1b) is valid, undergo a planar (i.e., one-dimensional) UAE. Ytrehus [7] argued that particles effusing from a porous wall into a vacuum behave in a similar way. Particles entering vacuum from a pulsed nozzle, on the other hand, would, as discussed in Sec. II B, evolve to a state which was more nearly axial than planar.

For planar, continuum flow, motion is governed by the pair of equations

$$\frac{\partial\rho}{\partial t}+\left[\frac{\partial}{\partial x}\right](\rho u)=0\ \text{(continuity equation)}\ , \tag{2a}$$

$$\frac{\partial u}{\partial t}+u\frac{\partial u}{\partial x}+(1/\rho)\left[\frac{\partial p}{\partial x}\right]=0\ \text{(Euler equation)}\ , \tag{2b}$$

where $\rho=mn$ is the particle mass density, p is pressure, and it is assumed that there is neither viscosity nor heat conduction. There is in principle a third equation [19,20,42]

$$\rho\frac{\partial e}{\partial t}+\rho u\frac{\partial e}{\partial x}+p\frac{\partial u}{\partial x}=\frac{\partial\Phi}{\partial x}\ \text{(energy equation)}\ , \tag{2c}$$

where e is the internal energy per unit mass and Φ (in the case of laser-pulse bombardment) is the laser heat input into the escaping particles in units of J/cm^2 s. In addition, we introduce the equation of state of a perfect gas,

$$p=nk_BT=\rho k_BT/m=\rho a^2/\gamma\ , \tag{3a}$$

and the condition for the adiabatic, reversible isentropic expansion of a perfect gas [49],

$$\rho\propto a^{2/(\gamma-1)}\ . \tag{3b}$$

Then it follows from the relation $a^2=(\partial p/\partial\rho)_S$, where S is entropy, that $\partial p/\partial x$ in Eq. (2b) is equal to $a^2\partial\rho/\partial x$. To simplify what follows we change to dimensionless variables:

$$X=x/u_K\tau_r,\quad \Upsilon=t/\tau_r,\quad A=a/u_K,\quad U=u/u_K\ ,$$

where τ_r is the length of the release process (not necessarily coincident with the laser pulse, whence the notation τ_r) or the duration of the nozzle being open. If there is no laser heat input, $\Phi=0$, then it is found with the help

of Eq. (3b) that the third basic relation, Eq. (2c), contains no separate information. This leaves Eqs. (2a) and (2b), which can be rewritten

$$\frac{\partial A}{\partial \Upsilon}+U\frac{\partial A}{\partial X}+\frac{(\gamma-1)A}{2}\frac{\partial U}{\partial X}=0 \quad \text{(continuity equation)}, \tag{4a}$$

$$\frac{\partial U}{\partial \Upsilon}+U\frac{\partial U}{\partial X}+\frac{2A}{\gamma-1}\frac{\partial A}{\partial X}=0 \quad \text{(Euler equation)}. \tag{4b}$$

B. Validity of the flow equations

There may appear to be a severe problem in the use of the flow equations, which assume local equilibrium, for an expansion which takes place into a vacuum and therefore leads to arbitrarily low densities. The usual way out of this contradiction is to assume that the flow equations remain valid until the density falls into a critical value and the particles go abruptly into free flight [4,15]. This approach, however, is not rigorous. We suggest that a powerful alternative for establishing to what extent the flow equations are useful is to compare the analytical solutions to be obtained here with the Boltzmann-equation results of Sibold and Urbassek [43]. The comparison is made, with favorable results, in Sec. VI C.

C. The flow phase

We will take the situation $M=1$ to apply abruptly at $X=\Upsilon=0$, so that the KL phase of the particle release (Sec. II) is represented as a boundary condition. The release which occurs in the interval $0\le\Upsilon\le 1$, and which will be termed the flow phase, is discussed here in Sec. III C. The gas-dynamic effects setting in abruptly at $\Upsilon>1$, and which will be termed the end-of-the-pulse phase, will be discussed in Secs. IV and V. Thus the desorption has so-called "top hat" form, assumed also by Sibold and Urbassek [43].

The solutions for the flow phase, assuming the flow to take place in vacuum, were previously [4] obtained by noting the close similarity with those for a one-dimensional "gun" with an infinite reservoir [50]. [The reservoir is infinite for the flow-phase solution seen in Eqs. (5) since only then is the problem of the reflection of the rarefaction wave avoided [4]. However, it is finite for outflow (Sec. I B).] In terms of our dimensionless variables the solutions are

$$A=1-\frac{\gamma-1}{\gamma+1}\frac{X}{\Upsilon}=1-\frac{X}{4\Upsilon}, \tag{5a}$$

$$U=1+\frac{2}{\gamma+1}\frac{X}{\Upsilon}=1+\frac{3X}{4\Upsilon}. \tag{5b}$$

In each of Eqs. (5) we give first the result for general γ and then the form for atoms with $\gamma=\frac{5}{3}$. This pattern will be followed throughout.

We have not yet commented on the fact that the surface of the target recedes. In the work of Srinivasan *et al.* [39,51], carried out at <10 J/cm^2, the typical extent of recession was <1 μm/pulse. For 500 K and $m=50$ u, a is about 4×10^4 cm/s so, in 20 ns, a gaseous disturbance would move about 8 μm. In view of the inequality 1 μm $\ll$ 8 μm, we see no reason to take the recession into account.

The material up to this point is straightforward in that it is a simple extension of ideas already worked out for an on-going planar UAE [4] resembling that for a gun being fired into vacuum [50]. Interestingly, the corresponding cylindrical and spherical problems are much more difficult and were only recently (and even then incompletely) solved [52].

IV. THE END-OF-THE-PULSE PHASE ($t\ge\tau_r$)

When the release process terminates at $\Upsilon=1$ the end-of-the-pulse phase begins and there is an abrupt change at $X=0$. Particles cease to flow out of the target (or nozzle, as is the case), from which it follows that the boundary condition changes suddenly either from $U=1$ to $U=0$ (absence of recondensation) or from $U=1$ to $U<0$ (presence of recondensation). We have chosen $U=0$ for the present work, a similar choice having been made by Knight [42] (Sec. VI B), whereas Sibold and Urbassek [43] chose $U<0$ (Sec. VI C). A further characteristic at $X=0$ will be seen to be a sudden change from $A=1$ to $0<A<1$, a condition supported by both numerical studies [42,43] and which we prove explicitly in what follows. It is unclear how to make a simple derivation of the consequences of the condition $X=U=0$, so we resort to what Stanyukovich (pp. 121, 151, and 170 of [50]) terms the "general solution."

The details of the "general solution" are outlined in Appendix B. The important relations for $\gamma=\frac{5}{3}$ are Eqs. (B1) (for all γ) and (B5) ($\gamma=\frac{5}{3}$), where ψ will be taken to have the form seen in Eq. (B7).

A. Region I: $0<X<X_I$

By introducing the condition $X=U=0$ into Eq. (B1), it follows that $\partial\psi/\partial U=0$. This suggests (though does not prove) that ψ for region I has the unusually simple form of Eq. (B10), so we have immediately

$$X=U\Upsilon \quad \text{(tentatively all } \gamma). \tag{6a}$$

Substitution of Eq. (6a) into Eqs. (4) now gives

$$A=L\Upsilon^{-(\gamma-1)/2}=L\Upsilon^{-1/3}, \tag{6b}$$

where any value of L is acceptable as far as Eqs. (4) are concerned but the correct value is as shown in Eq. (C1). We thus establish the correctness of the condition $0<A<1$ at $X=0$. In particular, the condition *is not* $A=0$, corresponding to the separation of the released particles from the surface as happens when the particles go directly into free flight [43].

The solutions seen in Eqs. (6) are tentatively valid for any γ from the surface at $X=0$ to the first *line of contact* (LOC) at X_I, i.e., for what we will call "region I." The validity is tentative because it is not clear that $\psi=C_0/A^m$, as in Eq. (B10), is the only possible solution.

B. Region II: $X_I < X < X_{II}$

The first LOC is the point of discontinuity where the solutions seen in Eqs. (6) (region I) meet what we will call "region II." Region II serves to join region I to the remanent of the flow phase, region III. To see this we note that any LOC moves with velocity

$$dX/d\Upsilon = U + A \ .$$

The first LOC therefore moves with a velocity appropriate to Eqs. (6), is located at

$$X_I = \frac{3-\gamma}{\gamma-1}(\Upsilon - \Upsilon^{(3-\gamma)/2}) = 2(\Upsilon - \Upsilon^{2/3}) \ , \tag{7a}$$

and is characterized by $A_I = L\Upsilon^{-(\gamma-1)/2}$, by $U_I = X_I/\Upsilon$, and by velocity $dX_I/d\Upsilon$. The second LOC, on the other hand, moves with a velocity appropriate to Eqs. (5), is located at

$$X_{II} = \frac{\gamma+1}{\gamma-1}(\Upsilon - \Upsilon^{(3-\gamma)/(\gamma+1)}) = 4(\Upsilon - \Upsilon^{1/2}) \ , \tag{7b}$$

and is characterized by velocity $dX_{II}/d\Upsilon$ and by the values

$$A_{II} = \Upsilon^{-2(\gamma-1)/(\gamma+1)} = \Upsilon^{-1/2} \ ,$$

$$U_{II} = \frac{\gamma+1}{\gamma-1} - \frac{2}{\gamma-1}\Upsilon^{-2(\gamma-1)/(\gamma+1)} = 4 - 3\Upsilon^{-1/2} \ .$$

It is clear that, except initially ($\Upsilon = 1$), the two LOC's are separate and the problem therefore has three regions.

The main obstacle in the present work was to find the solutions for region II, which we now do for atoms with $\gamma = \frac{5}{3}$. It is required that A and U for region II match in magnitude (although not slope) the solutions of regions I and III. Bearing in mind Eq. (B6) namely,

$$\psi = \frac{F(3A+U)}{A} \ , \tag{B6}$$

such matching is equivalent to the following four conditions: (a) $F'(2) = 0$ because of Eq. (B1) with X_I and U_I substituted for X and U, (b) $F'(4) = 1$ because of Eq. (B1) with X_{II} and U_{II} substituted for X and U, (c) $F(2) = -3A^3\Upsilon = -\frac{8}{9}$ because of Eq. (B5), and (d) $F(4) = 0$ because of Eq. (B5). Our method of making further progress is to propose a trial form for ψ which is simple yet mathematically acceptable. It is based on Eq. (B7):

$$\psi = \frac{C_3(3A+U)^3}{A} + \frac{C_2(3A+U)^2}{A} + \frac{C_1(3A+U)}{A} + \frac{C_0}{A} \ .$$

The four unknowns C_n are readily evaluated from the four conditions, the final result being

$$\psi = \frac{1}{36A}(3A+U)^3 - \frac{1}{3A}(3A+U) - \frac{4}{9A}, \quad C_2 = 0 \ . \tag{8}$$

We chose a series beginning with $n = 3$ because it was required by condition (c) and (with only four conditions) this made it possible to restrict ourselves to the n values 3, 2, 1, and 0.

The first part of the solution follows from Eqs. (B1) and (8) as

$$12AX = 12AU\Upsilon - (3A+U)^2 + 4 \tag{9a}$$

or

$$U = -3A + 6A\Upsilon - (36A^2\Upsilon^2 - 36A^2\Upsilon + 4 - 12AX)^{1/2} \ . \tag{9b}$$

The second part follows from Eqs. (B5) and (8) as

$$108A^3\Upsilon = -(3A+U)^3 + 9A(3A+U)^2 + 12U + 16 \ . \tag{9c}$$

C. Region III: $X_{II} < X < \hat{X}$

Region III is just a remanent of the flow phase seen in Eqs. (5). It begins at X_{II} and ends at $\hat{X}$, i.e., at the expansion front, given by introducing $A = 0$ in Eq. (5a):

$$\hat{X} = \frac{\gamma+1}{\gamma-1}\Upsilon = 4\Upsilon$$

and characterized by velocity

$$\hat{U} = \frac{\gamma+1}{\gamma-1} = 4 \ . \tag{10}$$

Values of A and U satisfying Eqs. (9) are summarized in Table III and shown graphically in Figs. 2–5. Perhaps the most important detail relates to the abrupt fall of the sound speed near the surface at $\Upsilon = 1$, as it implies an even more abrupt change in the density (column 3 of Table IV). Note how the density change is less marked for molecules than for atoms. We will argue in Sec. VI D that the density change can be seen in the photographs of Braren and co-workers [35,36]. We note also that the sound speed is at first spatially invariant, then increases

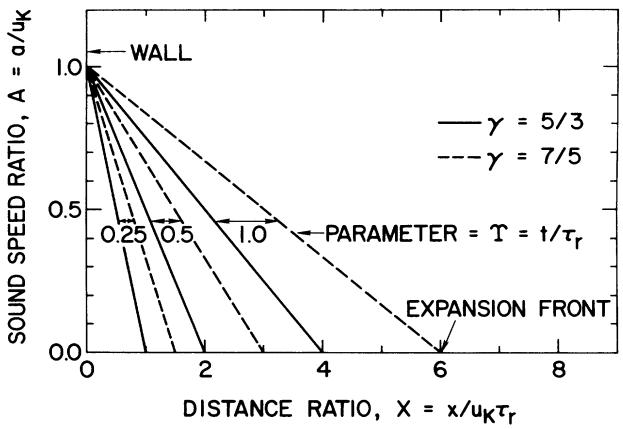

FIG. 2. Calculated values of sound speed ratio $A = a/u_K$ vs distance ratio $X = x/u_K\tau_r$ appropriate to the flow phase of laser-pulse sputtering for the effusion model. Here u_K is the flow velocity at the KL boundary and τ_r the length of the release process. At zero time ratio $\Upsilon = t/\tau_r = 0$ the wall of an infinite gas reservoir can be regarded as becoming suddenly porous and forming a KL [7], the outer boundary of which occurs at $X = 0$. The KL is thus approximated as a boundary condition. The A values should be governed by Eq. (5a) and are shown for two values of γ. The flow phase ends abruptly at time $\Upsilon = 1$, when the wall ceases to be porous.

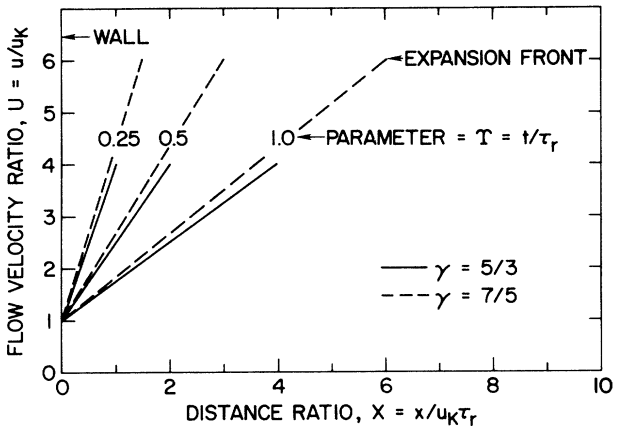

FIG. 3. Like Fig. 2 but showing flow velocity ratio $U=u/u_K$ vs distance ratio. The U values should be governed by Eq. (5b). Other details are as in Fig. 2.

with distance, and finally falls to zero at the expansion front. The existence of the invariant region as well as that where the sound speed increases (but to only a limited extent) should simplify the treatment of such problems as the passage to free flight, deriving temperatures from

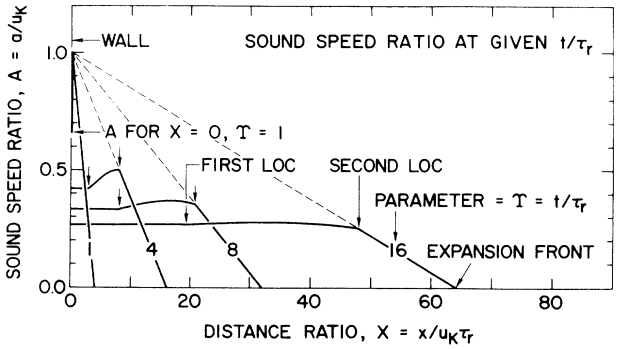

FIG. 4. Calculated values of sound speed ratio vs distance ratio appropriate to the end-of-the-pulse phase of laser-pulse sputtering for the effusion model. At $\Upsilon=1$ the previously porous wall at $X=0$ is suddenly sealed and as a result the boundary condition changes abruptly from $U=1$ to 0. The flow breaks up into three regions separated by two LOC's (marked variously with labeled or unlabeled arrows), region I being governed by Eq. (6b), II by Eqs. (9), and III by Eq. (5a). Region III is a remnant of the type of flow shown in Fig. 2, as can be inferred from the dashed lines. Note that the curve for $\Upsilon=1$ has a vertical segment at $X=0$ from $A=0.667$ to 1. The curves are for atoms with $\gamma=\frac{5}{3}$.

TABLE III. Values of A and U for region II obtained by trial-and-error solution of Eqs. (9). These equations apply to atoms with $\gamma=\frac{5}{3}$. For each value of Υ the first and last entries apply to the first and second LOC, as marked explicitly for $\Upsilon=1.1$.

Υ (time ratio)	X (distance ratio)	A (sound speed ratio)	U (flow velocity ratio)	Departure of A from linearity[a] (percent)
1.1	0.068 80 (X_{I})	0.6458 (A_{I})	0.062 54 (U_{I})	0.19
	0.1	0.7176	0.307 8	
	0.15	0.8311	0.703 0	
	0.2	0.9429	1.101 5	
	0.2048 (X_{II})	0.9535 (A_{II})	1.139 6 (U_{II})	
2	0.8252	0.5291	0.412 6	1.6
	1	0.5535	0.575 1	
	1.5	0.6180	1.048 2	
	2	0.6742	1.535 0	
	2.3431	0.7071	1.878 7	
4	2.9603	0.4200	0.740 1	3.3
	4	0.4464	1.088 3	
	5	0.4677	1.429 1	
	6	0.4844	1.776 6	
	7	0.4957	2.132 5	
	8	0.5	2.5	
8	8	0.3333	1	5.5
	10	0.3459	1.293 2	
	12	0.3558	1.589 6	
	14	0.3627	1.889 8	
	16	0.3660	2.194 7	
	18	0.3649	2.505 9	
	20.686	0.3536	2.939 3	
16	19.301	0.2646	1.206 3	8.0
	20	0.2659	1.254 1	
	28	0.2768	1.805 5	
	36	0.2783	2.367 0	
	44	0.2657	2.946 3	
	48	0.25	3.25	

[a] A is "convex up" to an extent which decreases as Υ decreases. For $\Upsilon=1+\Delta\Upsilon$, A can be taken as accurately linear, as assumed in Appendix C.

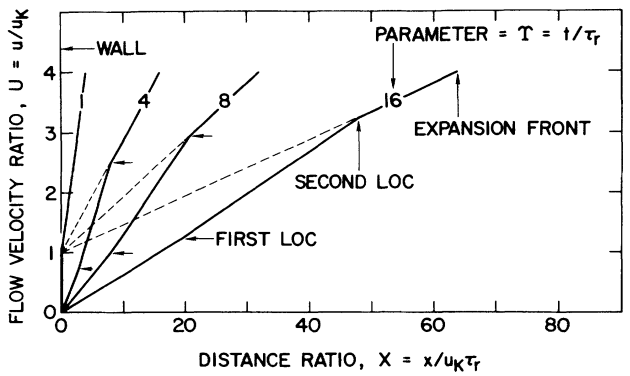

FIG. 5. Like Fig. 4 but showing flow velocity ratio vs distance ratio. The details are as in Fig. 4 except that region I is governed by Eq. (6a) and III by Eq. (5b). Note that the curve for $\Upsilon=1$ has a vertical segment at $X=0$ from $U=0$ to 1.

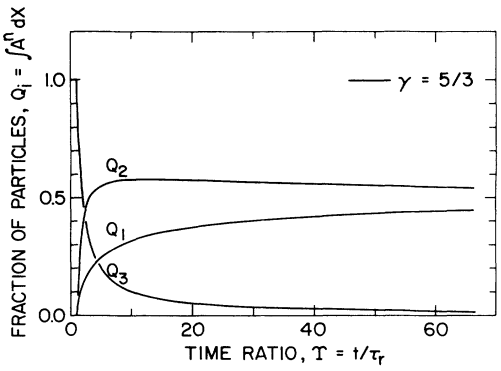

FIG. 6. Calculated values of the fraction of particles $Q_i=\int A^n dX$ present in each of the three regions seen in Figs. 4 and 5. $Q_{\rm I}$ is for $0<X<X_{\rm I}$, $Q_{\rm II}$ for $X_{\rm I}<X<X_{\rm II}$, $Q_{\rm III}$ for $X_{\rm II}<X<\hat{X}$, and n stands for $2/(\gamma-1)$. The curves, except that for $Q_{\rm III}$, are for atoms with $\gamma=\frac{5}{3}$; that for $Q_{\rm III}$ is more generally valid.

TOF spectra, and predicting condensation (i.e., cluster formation).

V. TOTAL QUANTITIES

For some applications, it is useful to know the fractions Q_i of particles present in each of the three regions, especially in the limit of large Υ. The method of obtaining the Q_i is basically to evaluate expressions of the type

$$Q_i=\int A^{2/(\gamma-1)}dX \ .$$

$Q_{\rm I}$, applying to $0<X<X_{\rm I}$, is the simplest. Referring to Eqs. (6b) and (7a) we have

$$\begin{aligned} Q_{\rm I}&=\left[\frac{3-\gamma}{2}\Upsilon^{-(\gamma-1)/2}\right]^{2/(\gamma-1)}X_{\rm I} \\ &=\frac{2}{\gamma-1}\left[\frac{3-\gamma}{2}\right]^{(\gamma+1)/(\gamma-1)}(1-\Upsilon^{-(\gamma-1)/2}) \\ &\equiv f(\gamma)(1-\Upsilon^{-(\gamma-1)/2}) \ , \end{aligned} \tag{11a}$$

where the factor $f(\gamma)$ equals $\frac{16}{27}$ for $\gamma=\frac{5}{3}$. This factor is equivalent to $Q_{\rm I}$ for large Υ.

$Q_{\rm III}$, applying to $X_{\rm II}<X<\hat{X}$, is also straightforward. Referring to Eq. (5a) we have

$$Q_{\rm III}=\int_{X_{\rm II}}^{\hat{X}}\left[1-\frac{\gamma-1}{\gamma+1}\frac{X}{\Upsilon}\right]^{2/(\gamma-1)}dX=\Upsilon^{-1} \ ,$$

a result that is accurately valid for all γ in spite of its simple form and which with $\Upsilon=1$ gives the total quantity

$$Q_{\rm total}=1 \ . \tag{11b}$$

$Q_{\rm II}$, applying to $X_{\rm I}<X<X_{\rm II}$, follows as the difference:

$$Q_{\rm II}=1-Q_{\rm I}-Q_{\rm III} \ .$$

The Q_i for $\gamma=\frac{5}{3}$ are shown in Fig. 6. The pattern that emerges is that the particles are roughly evenly divided between regions I and II, with the number in region III insignificant.

TABLE IV. Values of the quantities L, ρ/ρ_K, and m.

$\gamma=C_p/C_V$	The value of L in Eq. (C1)	The value of ρ/ρ_K for $X=0$, $\Upsilon=1$[a]	The exponent m in the relation $\psi=C_0/A^m$ [Eq. (B11)]
$\frac{5}{3}$	$\frac{2}{3}$	0.296	1
$\frac{7}{5}$	$\frac{4}{5}$	0.328	3
$\frac{9}{7}$	$\frac{6}{7}$	0.340	5
$\frac{11}{9}$	$\frac{8}{9}$	0.346	7

[a] ρ/ρ_K at $\Upsilon=1$ is given by $L^{2/(\gamma-1)}$. See Eqs. (3b) and (6b).

VI. COMPARISON WITH NUMERICAL AND EXPERIMENTAL WORK

A. Pulsed nozzles

Our analytical solution to the end-of-the-pulse phase is probably of no significant interest to most studies involving pulsed nozzles, at least with the present state of valve construction. This situation arises mainly because the times that valves are open are enormously longer than most laser pulses: 10–10 000 μs for valves [46–48] vs 10–30 ns for excimer lasers, yet the diameters of the released material are similar. As already seen in Table II, this means that the length-diameter ratio is 10^3–10^6 times greater for a pulsed nozzle expansion and the resulting geometry of the released material will tend to be axial rather than planar.

A less fundamental point is that the valves associated with nozzles are so mechanically imperfect that the gas-dynamic solutions presented here are probably too idealized. In laser-pulse sputtering, however, one encounters a nearly perfect and very rapid "valve." Consider a 20-ns pulse. Then, if an electronic mechanism is involved, the desorption probably starts within 1 or 2 ns, while for a thermal mechanism it starts near the end of the pulse when the temperature is near its maximum [53]. Similar-

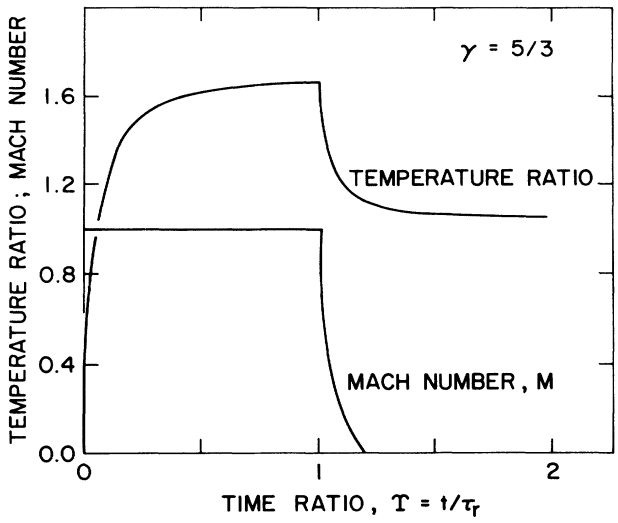

FIG. 7. Numerical solution of the flow equations [Eqs. (4)] by Knight [42] for laser-pulse sputtering. The situation considered was that of a rather long release pulse ($\tau_r = 1$ μs) delivering 10 J/cm^2 and directed against a solid surface having the thermal and optical properties of Al. Atoms with $\gamma = \frac{5}{3}$ were released thermally with a planar geometry. The temperature ratio $T/2730$ rises towards a steady-state value of 1.71. Its subsequent fall *does not* reflect the temperature of the gas, for which we would expect from Eqs. (1b) and (6b) a ratio 0.44 at $\Upsilon = 1.2$, but rather that of the solid surface. The Mach number M rises abruptly to unity, because the existence of a KL is taken as the boundary condition. It then falls to zero somewhat less than abruptly, the delay being due to the persisting vaporization which tracks the persisting temperature.

ly, the end of the desorption for an electronic process is normally thought to be abrupt (~20 ns in the present example) and that for thermal processes to be delayed only as is necessary for the temperature to fall. This delay can range from a fraction of the laser pulse length (Fig. 7) to much greater than the pulse length [sputtering of polymethylmethacrylate (PMMA) [35,36]].

B. Laser-pulse sputtering of aluminum: Knight [42] (Fig. 7)

Knight [42] solved the flow equations [Eqs. (4)] numerically for a problem very close to that treated here, the particles being atoms with $\gamma = \frac{5}{3}$. The greater part of the results relate to what we call the flow phase and which we previously [4] showed to be in good agreement with Eqs. (5). Important information on the end-of-the-pulse phase is, however, also available (Fig. 7). We note the following.

(a) Temperature. The temperature falls from $T/2730 = 1.68$ at $\Upsilon = 1$ to $T/2730 = 1.13$ at $\Upsilon = 1.2$, and then begins an on-going slow decrease. At first sight these results strongly disagree with what is expected. Thus, using the ratios $T_K/T_s = 0.669\,12$ from Sec. II A and $T/T_K = A^2 = (\frac{2}{3})^2(1.2)^{-2/3}$ from Eqs. (1b) and (6b), we expect $T/2730 = 0.44$ at $\Upsilon = 1.2$. The problem is that the temperature in Fig. 7 is that of the solid surface, and is the resultant of combined thermal conduction to the target interior and continued loss of energy to the vaporization which persists from $\Upsilon = 1$ to $\Upsilon \approx 1.2$. The gas temperature is very much lower.

(b) Mach number. The Mach number $M = u/a$ falls abruptly at $\Upsilon = 1$ though it does not reach zero until $\Upsilon \approx 1.2$. The delay is understandable in terms of the vaporization, thence the gas density, persisting briefly as the target surface cools. That $M = 0$ is finally reached agrees with our choice of boundary condition for region I, namely $X = U = 0$. It was an imposed result, however, in the sense that it did not follow automatically from the flow equations. Had recondensation been taken into account, then $M < 0$ would have been more appropriate.

(c) Pressure. It can also be shown that the pressure falls abruptly from 185 to about 30 atm at $\Upsilon = 1$, falls more slowly to ~4.2 atm at $\Upsilon \approx 1.2$ as the target surface cools, and then begins an on-going very slow decrease (Fig. 3 of [42]). The value that would be expected at $\Upsilon = 1.2$ according to the present work follows from two results: $p_K/p_s = 0.2062$ from Sec. II A and $p/p_K = A^5 = (\frac{2}{3})^5(1.2)^{-5/3}$ from Eqs. (3a) and (6b). We thus expect $p = 3.7$ atm, a value similar to that observed. This argument supports our choice $0 < A < 1$ at $X = 0$, and also shows that the gas cloud *does not detach* from the surface at $\Upsilon = 1$. (Note that the value 4.2 atm is only approximate as Fig. 3 of [42] is somewhat difficult to read.)

C. Pulsed desorption according to the Boltzmann equation: Sibold and Urbassek [43] [Figs. 8(a) and 8(b)]

Sibold and Urbassek [43] present Monte Carlo solutions of the Boltzmann equation for a problem close both to that of Knight [42] as well as to that treated here. They treated what we term the "recondensation" rather than "effusion" model in the sense that they permitted recondensation at the target surface when the release pulse terminated. Their results must therefore deviate from ours near the surface for $\Upsilon > 1$. Their approach automatically took into account the passage to free flight but not the KL, and this means not only that there will be disagreement near the surface for $\Upsilon \leq 1$, but also that normalizing the two sets of data will not be straightforward.

Concerning normalization, we have chosen to change the distance scale of [43] from $x/u_s\tau_r$ to $x/u_K\tau_r$ by means of the factor 1.324 [see Eqs. (1)]. The temperature scale of [43] was changed from T/T_s to T/T_K with the factor 0.669 12 (Sec. II A) and the flow-velocity scale from u/u_s to u/u_K with the aforementioned factor 1.324. These choices are justified empirically in that the results of [43] just beyond the surface (i.e., at the KL boundary) then coincide reasonably well with the analytical results. That is, coincidence at the KL boundary is more fundamental than coincidence at the surface.

The comparisons are shown in Fig. 8. We note the following.

(a) $\Upsilon = 1 - \delta$. Their results for $\Upsilon = 1 - \delta$ show the temperature [Fig. 8(a)], flow velocity [Fig. 8(b)], and density [3] to have values at the surface which disagree with ours,

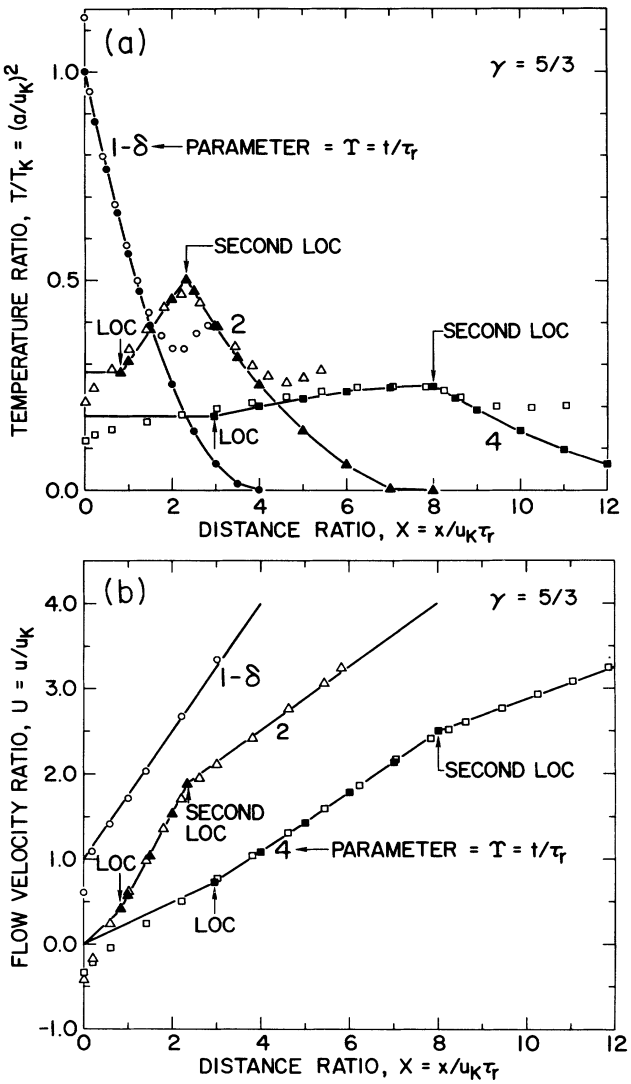

FIG. 8. Numerical solution of the Boltzmann equation by Sibold and Urbassek [43] for a problem close both to that of Knight [42] as well as to that treated here. The situation considered was that of an energetic pulse of particles directed against a target surface from which about 25 monolayers of atoms with $\gamma=\frac{5}{3}$ were released thermally with a planar geometry. The length of the release process was τ_r. Recondensation was permitted. We superimpose the numerical results of [43] (open points) with our analytical results as summarized in Table III (lines plus closed points, the points being used only for segments lacking rigorous linearity). (a) Temperature. There is general disagreement between [43] and our solutions at the very surface. Just beyond the surface, however, the points for $\Upsilon=1-\delta$ have the form expected from Eq. (5a) while the points for $\Upsilon=2$ and 4 have the form expected from Eqs. (6) and (9) except that the first LOC as well as region I are lacking. Note that what is marked as "LOC" is the *first LOC* and applies only to the analytical results, whereas *second LOC* applies to both sets of results. For large distances a new discrepancy sets in, in that the temperatures of [43] do not fall to zero. (b) Flow velocity. There is again disagreement between [43] and our solutions at the very surface, the u values of [43] being either low or negative. Just beyond the surface, however, all points have the values expected from Eqs. (5b), (6), and (9). There is no discrepancy for large distances like that seen in (a).

a disagreement which is to be expected when the KL is not taken into account: T and ρ are too high, u is too low. Nevertheless, starting *just beyond the surface* there is in all cases unusually good agreement between the two approaches. Except for temperature, this agreement persists to the largest distances considered.

For large distances the density falls to zero [3], as it should, but the temperature does not [Fig. 8(a)]. This unusual result is described [43] as being due to a lack of equilibrium at lower densities, thence lack of validity of the flow equations, such that the temperature parallel to the flow falls but that perpendicular to the flow increases. Similar results were obtained earlier in analytical solutions to the Boltzmann and moment equations in the asymptotic limit [23,41].

(b) $\Upsilon=2$ *and 4.* Their results at $X=0$ for $\Upsilon=2$ and 4 show the temperature, flow velocity, and density to have values at the surface which disagree with ours: T and ρ are too low, u is negative. The reason this time for a discrepancy is not that the KL was neglected, as there is no KL for $\Upsilon>1$, but rather that different surface boundary conditions were used. In [43] the condition, for $\Upsilon>1$, was $U<0$ while in our work it was $U=0$. Nevertheless, starting at the *first LOC* (marked in Fig. 8 and in [3] simply "LOC") there is again unusually good agreement between the two approaches.

(c) The LOC. Figures 8(a) and 8(b) clearly show the second LOC. The first LOC, as well as the existence of region I and its spatially invariant sound speed (thence temperature and density), are, on the other hand, not reproduced. The authors explain this as being a natural result when particles incident on the surface are absorbed (recondensed) instead of reflected [54].

(d) Detachment. For such low gas densities that a gas-dynamic description is not appropriate and the initial distribution (whether Maxwellian or otherwise) persists, they found for $\Upsilon>1$ and $X=0$ the boundary condition $\rho=T=U=0$. It follows that the gas cloud has detached from the surface. This is a fundamental difference from the high-density case, where the boundary conditions include $0<A<1$ and the gas cloud therefore *does not detach* [Fig. 8(a)].

D. Photographs of the sputtering of PMMA: Braren, Casey, and Kelly [35] [Figs. 9(a)–9(c)]

Various authors have sputtered either the polymer PMMA [33,35,36] or biological tissue [40] in air at 1 atm with ~20-ns laser pulses at 193 and 248 nm and have taken high-speed photographs of the emission process by firing above the target a second laser (e.g., 1 ns at 596 nm [35]) with a known delay. They confirmed a column of heavy particles (here called "ejecta") and a nearly hemispherical shock wave. Because of the presence of air, the leading edge of the ejecta constituted not an *expansion front* [Eq. (10)], but a *contact front* [8,49]. Hemispherical shock waves are well known both in laser sputtering [33–36,55] and in explosions [56], but are not otherwise relevant in the present context.

The conclusion of these [33,35,36,40] and other [38,57] studies of PMMA or tissue sputtering is that the laser

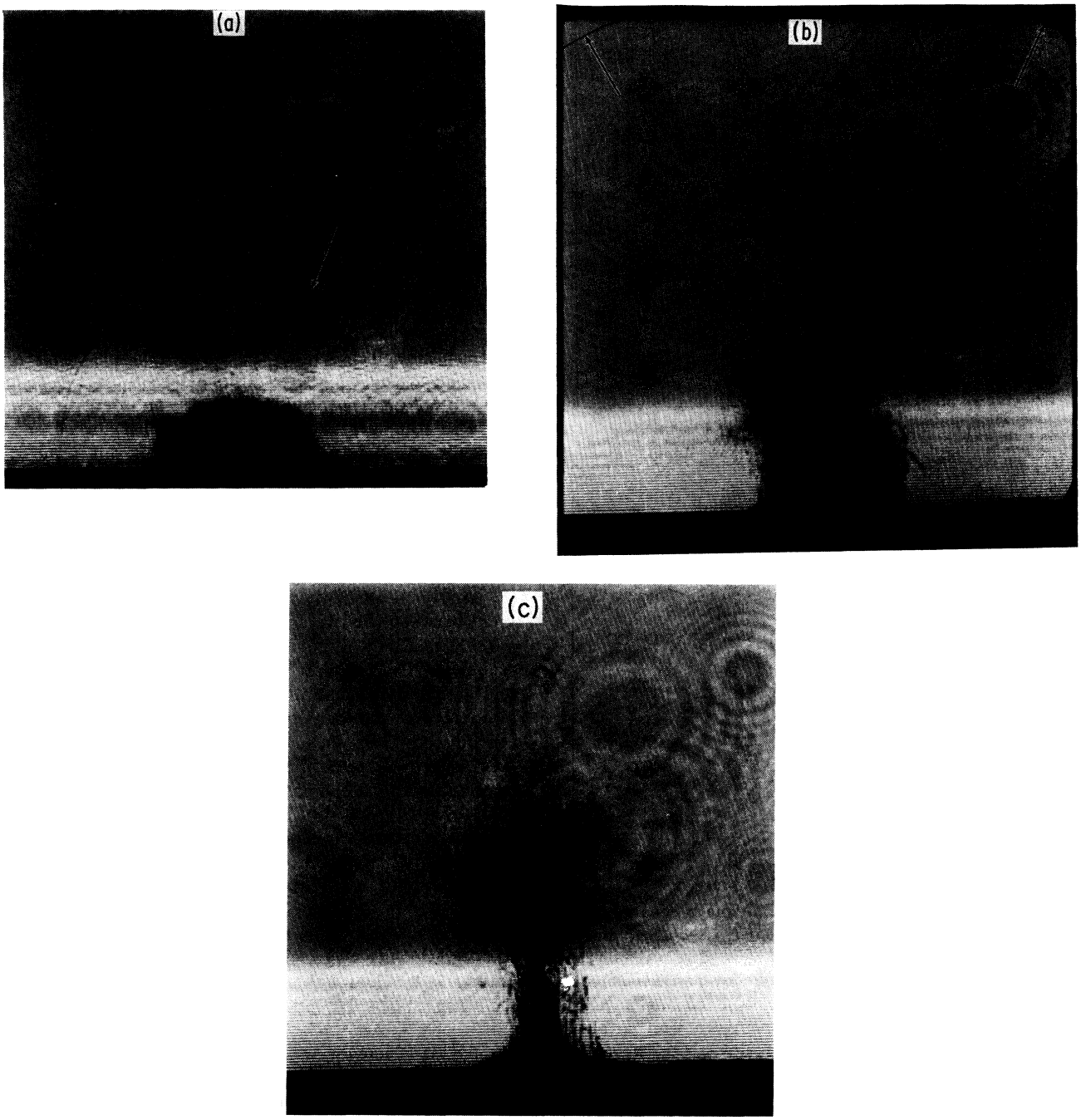

FIG. 9. Explicit photography of laser-pulse sputtered PMMA by Braren, Casey, and Kelly [35]. PMMA targets with a thickness of 0.7 mm were exposed to single laser pulses (2 J/cm^2, 248 nm, $\sim$20 ns, diameter $=$970 μm) in air. The ejecta were photographed by firing above the target a second laser (596 nm, $\sim$1 ns) with a known delay and thereby imaging both the ejecta and the shock wave. All features that would either absorb or scatter are seen, although there appears to be an imaging threshold. (a) Delay of 1 μs. We recognize a column of ejecta having the width of the laser-irradiated area, an extension of 0.42 mm, and a somewhat ill-defined leading edge. The average velocity is 4.2×10^4 cm/s. There is also a nearly hemispherical shock wave, marked with an arrow, having an extension of 1.2 mm. The average velocity of the shock wave is 12×10^4 cm/s, which is, as it must be [3,49], greater than that of the leading edge. (b) Delay of 6 μs. The column of ejecta still has the width of the laser-irradiated area, an extension of 1.0 mm, and an average velocity of 1.7×10^4 cm/s. The shock wave, marked with arrows at the top of the photograph, has an extension of 3.3 mm and an average velocity of 5.6×10^4 cm/s. (c) Delay of 15 μs. Near the target surface the column of ejecta has suffered an abrupt loss of density and, in addition, is imaged preferentially towards the axis. According to Fig. 4 and the corresponding figure for the outflow model [2], the density change would begin at the target surface and progress as a LOC. The ejecta far from the surface have a width slightly greater than that of the laser-irradiated area, the extension is 1.8 mm, and the average velocity is 1.2×10^4 cm/s. A shock wave is still present, but is far beyond the field of view.

pulses are absorbed within a characteristic depth and particles are released. A selection of explicit images from [35] is reproduced in Fig. 9 and we recall at this point that there are various limiting categories of gas-dynamic behavior as discussed in Secs. I A and I B. If the release is from the target surface, then there will be a combined KL-UAE, the description of which in the absence of recondensation is the object of this article (effusion model). A similar process exists also in the presence of recondensation (recondensation model [3]). If instead there is rapid bond breakage, the system is subject to outflow from a finite reservoir (outflow model [2]).

We note the following.

(a) Radial expansion. The radial expansion of the ejecta is quite limited for up to 15 μs [Fig. 9(c)], showing that a planar geometry as assumed here is acceptable. The real geometry is, however, probably intermediate between planar and axial. The existence of a near-planar geometry is equivalent to laser-sputtered particles showing strong forward peaking [26].

(b) The density "catastrophe." Between 6 [Fig. 9(b)] and 9 μs (not shown) the column of ejecta shows a remarkable change in which it loses density near the target surface. Our interpretation [35] is that the pulse length relevant to the sputtering (τ_r) is not the $\sim$20-ns duration of the laser pulse but more nearly $\sim$6 μs, during which there is ongoing release of debris from the PMMA surface. At $\sim$6 μs the release process ceases and we arrive at the situation $\Upsilon=1$, thence an abrupt decrease in density at the target surface as in column 3 of Table IV. We argue [35] that, since 6 μs is similar to the heat retention time constant, the relevant model is effusion or recondensation rather than outflow. This is because the latter would have been governed by a much shorter time constant, essentially

$$\tau_s = 2d_{\text{crater}}/a_4 \approx 150 \text{ ns} ,$$

where d_{crater} is the crater depth and a_4 the speed of sound in the reservoir. It follows that Fig. 4 is relevant, according to which the reduced density begins at the surface and ends with the *second* LOC.

(c) Perpendicular density variation. The photographs fail to record the rapid decrease in density to be expected for $\Upsilon<1$ (Fig. 2). This result is believed to be a consequence of the ejecta being largely opaque near the surface, so that density variations are not sensed, and not being imaged at all for the lower densities near the contact front [35]. In effect, there is an imaging threshold.

The photographs do, on the other hand, show that density *increases with distance* for $\Upsilon>1$ and that the increase begins near the middle of the column of ejecta at 15 μs. These are natural results for the effusion or recondensation model [Fig. 4 and Eqs. (7)] but do not occur for outflow [2]. Altogether, the relevance of the former models is indicated in three ways: (i) the value $\sim$6 μs for the release time constant τ_r; (ii) the tendency, for $\Upsilon>1$, for density to *increase with distance;* and (iii) the fact that the density increase begins the middle of the column of ejecta [Eqs. (7)].

(d) Detachment. For times from 9 to $\sim$30 μs the ejecta remained "attached" to the surface as they expanded, in accordance both with our Fig. 4 and with the numerical solutions [42,43]. This suggests ongoing gas-dynamic interactions which could be said to create a column of ejecta which simply "stretched" with time.

E. Angular effects in the sputtering of CdS: Namiki, Kawai, and Ichige [26] (Fig. 1)

We showed in Fig. 1 an example of the dependence of the *apparent* TOF temperature (T_s^{app}) on the ejection polar angle for laser-pulse sputtering of CdS [26]. Reference to Fig. 8 of [4], but with information for $\gamma=\frac{7}{5}$ and $\frac{9}{7}$ instead of $\frac{5}{3}$, enables values of M to be deduced. For 0° ejection angle M varies from 0 to 4–5 as the fluence increases, while for 15° the range is 0 to 3–4. At 45°, on the other hand, the results are not compatible with the laws of ideal gas dynamics in that T_s^{app} should not have decreased.

In the same study the angular variation of the yields of S_2 and Cd for a fluence of 0.036 J/cm^2 were shown to have the approximate form $\cos^{25}\theta$. Reference to Fig. 4 of [4], but with information for $\gamma=\frac{7}{5}$ and $\frac{9}{7}$ instead of $\frac{5}{3}$, shows that the corresponding value of M is $M\approx4$.

We regard the internal consistency as reasonable. Historically, it was existence of such results as these that was the first indication that laser-sputtered particles underwent a UAE [11,27].

F. Energy distributions: Namiki, Kawai, and Ichige [26] and NoorBatcha, Lucchese, and Zeiri [5,6]

In experiments such as those of [26] and in simulations such as those of [5,6], among the quantities measured were energy spectra. An approximate energy spectrum can be deduced consistent with the effusion model. We note from Fig. 4 that, for large Υ, the profile of sound speed versus distance becomes flat in regions I and II, and from Fig. 6 that only these regions are important. A very similar problem was discussed previously in connection with systems showing outflow. One postulates the existence of a critical density at which free flight occurs. Then the entirety of regions I and II will, at a certain value of Υ, enter into free flight. The particles will have a uniform temperature and, to reasonable approximation, a linearly increasing distribution of flow velocities (Fig. 5). The result is Eq. (9) of [2], an expression which can be shown to be indistinguishable in width from either a true Maxwellian or a Maxwellian with flow, at least for normally emitted particles and with proper respect for the error bars.

As far as the experimental spectra are concerned, those measured for normally emitted particles were indeed Maxwellian in form [26]. The shapes assumed by energy spectra are thus not a good test of the role of gas dynamics in sputtering.

ACKNOWLEDGMENTS

The author benefited greatly from discussions with B. Braren and K. G. Casey of IBM. These people made a

point of showing the relevance of their recent experimental work to the present gas-dynamic arguments. H.M. Urbassek (Technische Universität, Braunschweig, Germany) contributed discussions, arguments, numerical results, and a copy of [43] prior to publication. Equally important, he located an error whereby we had claimed that a simple power series like Eq. (B7) held also for $\gamma < 5/3$. [The real form is somewhat more complicated, as in Eq. (B9).] C. J. Knight (Avco Research, Everett, MA) discussed [42] and provided a FORTRAN code for solving the flow equations. A. Vertes (George Washington University, Washington, DC) contributed arguments and sent copies of [19,20] prior to publication. A. Miotello (University of Trento, Povo, Trento, Italy) is in the process of making a numerical test of the solutions obtained here [60].

APPENDIX A: NOTATION

Difficulties arose in this work because of the lack of a uniform notation for thermodynamic quantities at the target surface and at the KL boundary. We therefore summarize in Table I the usages in the present work along with with Refs. [3,4,7,10,43].

APPENDIX B: ON THE "GENERAL SOLUTION" OF STANYUKOVICH [50]

Equations (4) have as independent variables X and Υ. They are transformed by first making A and U the independent variables. We take the result of p. 121 of [50], but with the variable changed from the enthalpy H (i in the notation of [50]) to the sound speed a using the relation $H = a^2/(\gamma-1)$:

$$\frac{\partial X}{\partial U} - U\frac{\partial \Upsilon}{\partial U} + \frac{(\gamma-1)A}{2}\frac{\partial \Upsilon}{\partial A} = 0 \quad \text{(continuity equation)} ,$$

$$\frac{\partial X}{\partial A} - U\frac{\partial \Upsilon}{\partial A} + \frac{2A}{\gamma-1}\frac{\partial \Upsilon}{\partial U} = 0 \quad \text{(Euler equation)} .$$

A second transformation results by introducing the ansatz

$$X = U\Upsilon - \frac{\partial \psi}{\partial U} \quad \text{(all } \gamma) , \tag{B1}$$

namely

$$\frac{3-\gamma}{(\gamma-1)A}\frac{\partial \psi}{\partial A} - \left[\frac{2}{\gamma-1}\right]^2 \frac{\partial^2 \psi}{\partial U^2} + \frac{\partial^2 \psi}{\partial A^2} = 0$$

$$\text{(continuity equation)} , \tag{B2}$$

$$\frac{2A\Upsilon}{\gamma-1} = \frac{\partial \psi}{\partial A} \quad \text{(Euler equation)} . \tag{B3}$$

For atoms with $\gamma = \frac{5}{3}$ the above equations become

$$\frac{2}{A}\frac{\partial \psi}{\partial A} - 9\frac{\partial^2 \psi}{\partial U^2} + \frac{\partial^2 \psi}{\partial A^2} = 0 , \tag{B4}$$

$$3A\Upsilon = \frac{\partial \psi}{\partial A} . \tag{B5}$$

It is important to note that in Eqs. (B1)–(B5), since A and U are independent variables, we have $\partial U/\partial A = \partial A/\partial U = 0$.

Equation (B4) is satisfied in general by

$$\psi = \frac{F(3A+U)}{A} \quad (\gamma = \tfrac{5}{3}) , \tag{B6}$$

where the function $F(3A+U)$ must be determined, as well as by

$$\psi = \sum_n \frac{C_n(3A+U)^n}{A} + \frac{C_0}{A} \quad (\gamma = \tfrac{5}{3}) , \tag{B7}$$

where C_n and C_0 are constants and n is unrestricted. These solutions are easily shown to be acceptable by substitution into Eq. (B4), but we do not know whether Eq. (B7) is less general than (B6).

For $\gamma < \frac{5}{3}$, ψ is more complicated (pp. 151 and 170 of [50]). For example, for $\gamma = \frac{7}{5}$, instead of Eq. (B6) we find

$$\psi = \frac{F'(5A+U)}{A^2} - \frac{F(5A+U)}{5A^3} \quad (\gamma = \tfrac{7}{5}) , \tag{B8}$$

and instead of Eq. (B7) we find

$$\psi = \sum_n \frac{5nC_n(5A+U)^{n-1}}{A^2} - \sum_n \frac{C_n(5A+U)^n}{A^3} + \frac{C_0}{A^3}, \quad (\gamma = \tfrac{7}{5}) , \tag{B9}$$

as is easily shown by substituting Eqs. (B8) and (B9) in (B2). More generally, as γ decreases, ψ becomes an increasingly complicated function of $F(2A/(\gamma-1)+U)$ and its derivatives. Nevertheless, a *tentative* value of ψ for region I is easy to establish. The condition $X = U = 0$ can be taken as showing, as already argued in connection with Eq. (6a), that $F(2A/(\gamma-1)+U)$ is constant, leading to

$$\psi = C_0/A^m \quad \text{(tentatively all } \gamma) . \tag{B10}$$

Substitution of Eq. (B10) into (B2) fixes m:

$$m = 2(2-\gamma)/(\gamma-1) , \tag{B11}$$

with values as in Table IV. Substitution of Eq. (B10) into (B3) yields

$$A^{m+2}\Upsilon = -m(\gamma-1)C_0/2 = -(2-\gamma)C_0 .$$

But since we have $A = L\Upsilon^{-(\gamma-1)/2}$, C_0 can be finally evaluated explicitly:

$$C_0 = -\frac{1}{2-\gamma}L^{2/(\gamma-1)} \quad \text{(tentatively all } \gamma) . \tag{B12}$$

We emphasize that Eqs. (B10)–(B12) are *tentative*. They will be considered again elsewhere, with the question being asked whether Eqs. (B10)–(B12) are the only possible solution to the condition $X = U = 0$ [60].

APPENDIX C: ON THE RELATION $A = L\Upsilon^{-(\gamma-1)/2}$

We have already noted in Sec. IV A that any value of L is acceptable as far as Eqs. (4) are concerned. The true

value of L can be obtained by conserving the number of particles for a time near $\Upsilon=1$, namely $\Upsilon=1+\Delta\Upsilon$, when A for region II is accurately linear (column 5 of Table III). $Q_{\rm I}$ is given by

$$Q_{\rm I}=A^{2/(\gamma-1)}X_{\rm I}\approx L^{(\gamma+1)/(\gamma-1)}\Delta\Upsilon \ ,$$

where $X_{\rm I}$ has been written in the form with explicit L, i.e., not Eq. (7a) but

$$X_I=\frac{2L}{\gamma-1}(\Upsilon-\Upsilon^{(3-\gamma)/2}) \ .$$

Since A within $X_{\rm I}<X<X_{\rm II}$ is linear, we have for $Q_{\rm II}$

$$Q_{\rm II}=\int_{X_{\rm I}}^{X_{\rm II}}\left[A_I+\frac{1-A_{\rm I}}{X_{\rm II}-X_{\rm I}}[X-X_{\rm I}]\right]^{2/(\gamma-1)}dX$$
$$\approx\frac{(\gamma-1)(2-L)(1-L^{(\gamma+1)/(\gamma-1)})}{(1-L)(\gamma+1)}\Delta\Upsilon \ .$$

Finally, the fraction $Q_{\rm III}$ contained within $X_{\rm II}<X<\hat{X}$ is

$$Q_{\rm III}=\int_{X_{\rm II}}^{\hat{X}}A^{2/(\gamma-1)}dX=\Upsilon^{-1}\approx 1-\Delta\Upsilon \ .$$

By requiring conservation of particles, $Q_{\rm I}+Q_{\rm II}+Q_{\rm III}=Q_{\rm total}=1$ [Eq. (11b)], it follows without difficulty that L is given by

$$L=\frac{3-\gamma}{2}=\frac{2}{3} \ , \qquad \text{(C1)}$$

with values as in Table IV.

Note that L is not zero, a result that is supported both by the numerical treatments [42,43] (Figs. 7 and 8) and by the photographs [35,36] (Fig. 9). $L=0$ might have been chosen to accommodate the sudden cessation of flow at $X=0$ at instant $\Upsilon=1$, but is wrong.

---

*This work was completed during a visit to the Dipartimento di Scienze Chimiche, Università di Catania, Viale A. Doria 6, 95125 Catania, Italy.

[1] H. M. Urbassek and J. Michl, Nucl. Instrum. Methods B **22**, 480 (1987).
[2] R. Kelly, Nucl. Instrum. Methods B **46**, 441 (1990).
[3] R. Kelly and B. Braren, Appl. Phys. B **53**, 160 (1991).
[4] R. Kelly, J. Chem. Phys. **92**, 5047 (1990).
[5] I. NoorBatcha, R. R. Lucchese, and Y. Zeiri, J. Chem. Phys. **86**, 5816 (1987).
[6] I. NoorBatcha, R. R. Lucchese, and Y. Zeiri, J. Chem. Phys. **89**, 5251 (1988).
[7] T. Ytrehus, in *Rarefied Gas Dynamics,* edited by J. L. Potter (AIAA, New York, 1977), p. 1197.
[8] C. J. Knight, AIAA J. **17**, 519 (1979).
[9] D. A. Labuntsov and A. P. Kryukov, Int. J. Heat Mass Transfer **22**, 989 (1979).
[10] C. Cercignani, in *Rarefied Gas Dynamics,* edited by S. S. Fisher (AIAA, New York, 1981), p. 305.
[11] R. Kelly and R. W. Dreyfus, Surf. Sci. **198**, 263 (1988).
[12] R. Kelly and R. W. Dreyfus, Nucl. Instrum. Methods B **32**, 341 (1988).
[13] R. Kelly, *Desorption Induced by Electronic Transitions, DIET IV* (Springer-Verlag, Heidelberg, 1990), p. 135.
[14] R. Schilder, G. Adomeit, and G. Wortberg, in *Rarefied Gas Dynamics,* edited by O. M. Belotserkovskii *et al.* (Plenum, New York, 1985), p. 577.
[15] K. L. Saenger, J. Chem. Phys. **75**, 2467 (1981).
[16] T. Venkatesan, X. D. Wu, A. Inam, and J. B. Wachtman, Appl. Phys. Lett. **52**, 1193 (1988).
[17] G. Koren, A. Gupta, R. J. Baseman, M. I. Lutwyche, and R. B. Laibowitz, Appl. Phys. Lett. **55**, 2450 (1989).
[18] G. Koren, R. J. Baseman, A. Gupta, M. I. Lutwyche, and R. B. Laibowitz, Appl. Phys. Lett. **56**, 2144 (1990); **57**, 1169 (1990).
[19] A. Vertes, P. Juhasz, M. de Wolf, and R. Gijbels, Int. J. Mass Spectrom. Ion Processes **94**, 63 (1989).
[20] L. Balazs, R. Gijbels, and A. Vertes, Anal. Chem. **63**, 314 (1991).
[21] M. M. Martynyuk, Russ. J. Phys. Chem. **57**, 494 (1983).
[22] R. Mager, G. Adomeit, and G. Wortberg, in *Rarefied Gas Dynamics,* edited by Muntz *et al.* (AIAA, Washington, DC, 1990), p. 461.
[23] R. E. Grundy, Phys. Fluids **12**, 2011 (1969).
[24] F. S. Sherman, Lockheed Missiles and Space Co. Report No. 6-90-63-61, 1963 (unpublished).
[25] H. Ashkenas and F. S. Sherman, in *Rarefied Gas Dynamics,* edited by de Leeuw (Academic, New York, 1966), Vol. II, p. 84.
[26] A. Namiki, T. Kawai, and K. Ichige, Surf. Sci. **166**, 129 (1986).
[27] J. P. Cowin, D. J. Auerbach, C. Becker, and L. Wharton, Surf. Sci. **78**, 545 (1978).
[28] E. B. D. Bourdon, P. Das, I. Harrison, J. C. Polanyi, J. Segner, C. D. Stanners, R. J. Williams, and P. A. Young, Chem. Soc. Faraday Disc. **82**, 1 (1986).
[29] A. Frezzotti, in *Rarefied Gas Dynamics,* edited by V. Boffi and C. Cercignani (Teubner, Stuttgart, 1986), p. 313.
[30] H. M. Urbassek, Nucl. Instrum. Methods B **31**, 541 (1988).
[31] C. H. Becker and J. B. Pallix, J. Appl. Phys. **64**, 5152 (1988).
[32] C. E. Otis, Appl. Phys. B **49**, 455 (1989).
[33] R. Srinivasan, B. Braren, K. G. Casey, and M. Yeh, Appl. Phys. Lett. **55**, 2790 (1989).
[34] R. Srinivasan, K. G. Casey, and B. Braren, Chemtronics **4**, 153 (1989).
[35] B. Braren, K. G. Casey, and R. Kelly, Nucl. Instrum. Methods B **58**, 463 (1991).
[36] R. Kelly, A. Miotello, B. Braren, A. Gupta, and K. Casey, Nucl. Instrum. Methods B **65**, 187 (1992).
[37] A. Namiki, K. Katoh, Y. Yamashita, Y. Matsumoto, H. Amano, and I. Akasaki, J. Appl. Phys. **70**, 3268 (1991).
[38] B. J. Garrison and R. Srinivasan, J. Appl. Phys. **57**, 2909 (1985).
[39] R. Srinivasan, B. Braren, and R. W. Dreyfus, J. Appl. Phys. **61**, 372 (1987).
[40] C. A. Puliafito, D. Stern, R. R. Krueger, and E. R. Mandel, Arch. Ophthalmol. **105**, 1255 (1987).
[41] B. B. Hamel and D. R. Willis, Phys. Fluids **9**, 829 (1966).
[42] C. J. Knight, AIAA J. **20**, 950 (1982).

[43] D. Sibold and H. M. Urbassek, Phys. Rev. A **43**, 6722 (1991).
[44] R. W. Dreyfus, R. Kelly, and R. E. Walkup, Nucl. Instrum. Methods B **23**, 557 (1987).
[45] R. W. Dreyfus, R. Kelly, and R. E. Walkup, Appl. Phys. Lett. **49**, 1478 (1986).
[46] K. L. Saenger, J. Chem. Phys. **79**, 6043 (1983).
[47] W. R. Gentry and C. F. Giese, Rev. Sci. Instrum. **49**, 595 (1978).
[48] F. M. Behlen and S. A. Rice, J. Chem. Phys. **75**, 5672 (1981).
[49] H. W. Liepmann and A. Roshko, *Elements of Gasdynamics* (Wiley, New York, 1957), pp. 13, 49, and 80.
[50] K. P. Stanyukovich, *Unsteady Motion of Continuous Media* (Pergamon, London, 1960).
[51] R. Srinivasan, B. Braren, R. W. Dreyfus, L. Hadel, and D. E. Seeger, J. Opt. Soc. Am. A **3**, 785 (1986).
[52] R. F. Schmalz, Phys. Fluids **28**, 2923 (1985).
[53] R. Kelly and J. E. Rothenberg, Nucl. Instrum. Methods B **7/8**, 755 (1985).
[54] H. M. Urbassek (private communication).
[55] J. L. Bobin, Y. A. Durand, Ph. P. Langer, and G. Tonon, J. Appl. Phys. **39**, 4184 (1968).
[56] D. A. Freiwald and R. A. Axford, J. Appl. Phys. **46**, 1171 (1975).
[57] S. Küper and M. Stuke, Appl. Phys. B **44**, 199 (1987).
[58] P. Simon, Appl. Phys. B **48**, 253 (1989).
[59] F. P. Gagliano and U. C. Paek, Appl. Opt. **13**, 274 (1974).
[60] A. Miotello and R. Kelly (unpublished).

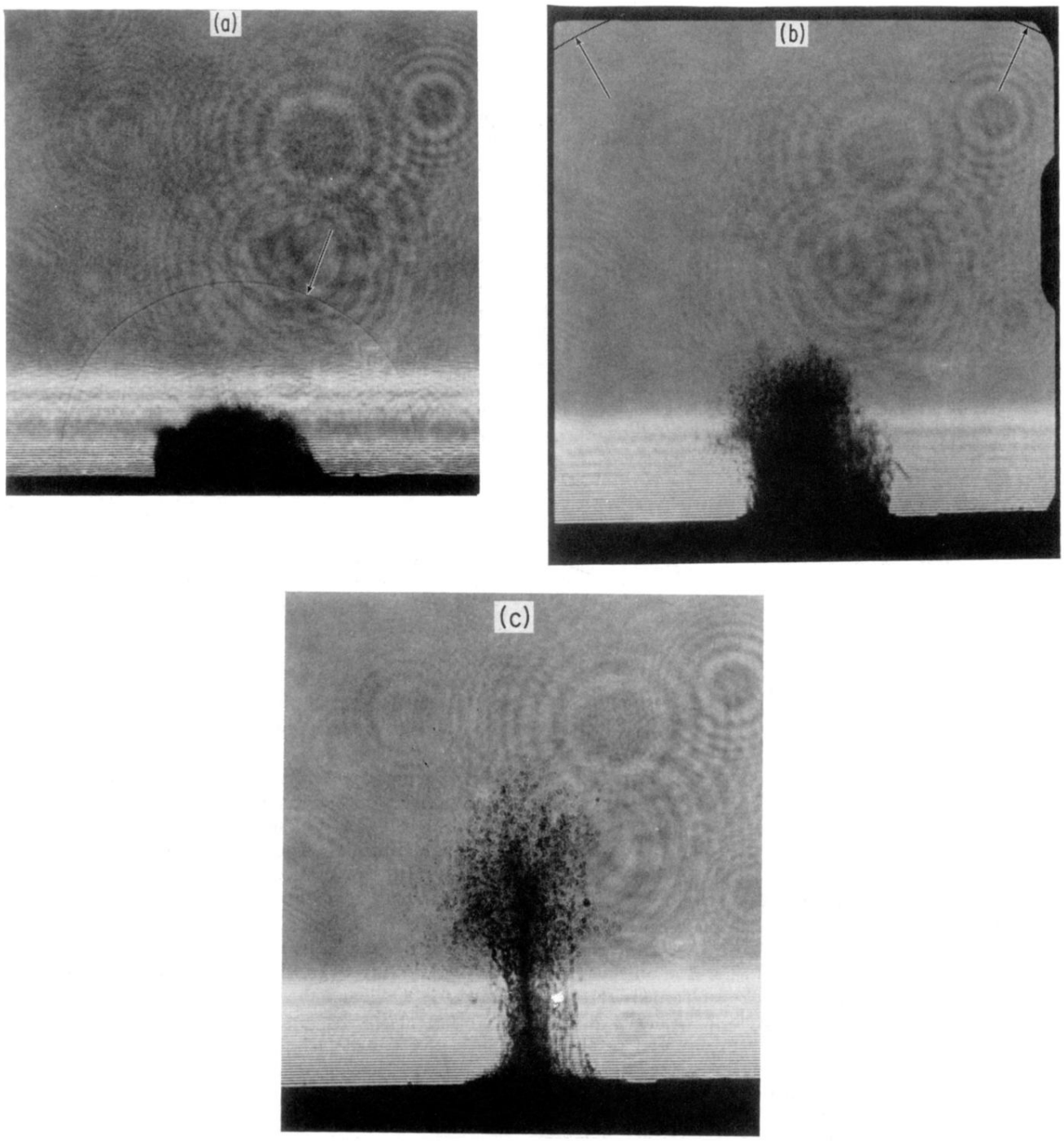

FIG. 9. Explicit photography of laser-pulse sputtered PMMA by Braren, Casey, and Kelly [35]. PMMA targets with a thickness of 0.7 mm were exposed to single laser pulses (2 J/cm^2, 248 nm, $\sim$20 ns, diameter $=$970 μm) in air. The ejecta were photographed by firing above the target a second laser (596 nm, $\sim$1 ns) with a known delay and thereby imaging both the ejecta and the shock wave. All features that would either absorb or scatter are seen, although there appears to be an imaging threshold. (a) Delay of 1 μs. We recognize a column of ejecta having the width of the laser-irradiated area, an extension of 0.42 mm, and a somewhat ill-defined leading edge. The average velocity is 4.2×10^4 cm/s. There is also a nearly hemispherical shock wave, marked with an arrow, having an extension of 1.2 mm. The average velocity of the shock wave is 12×10^4 cm/s, which is, as it must be [3,49], greater than that of the leading edge. (b) Delay of 6 μs. The column of ejecta still has the width of the laser-irradiated area, an extension of 1.0 mm, and an average velocity of 1.7×10^4 cm/s. The shock wave, marked with arrows at the top of the photograph, has an extension of 3.3 mm and an average velocity of 5.6×10^4 cm/s. (c) Delay of 15 μs. Near the target surface the column of ejecta has suffered an abrupt loss of density and, in addition, is imaged preferentially towards the axis. According to Fig. 4 and the corresponding figure for the outflow model [2], the density change would begin at the target surface and progress as a LOC. The ejecta far from the surface have a width slightly greater than that of the laser-irradiated area, the extension is 1.8 mm, and the average velocity is 1.2×10^4 cm/s. A shock wave is still present, but is far beyond the field of view.